Taming Phosphorus Mononitride (PN)

André K. Eckhardt,[a] Martin-Louis Y. Riu,[a] Mengshan Ye,[a] Peter Müller,[a] Giovanni Bistoni,[b] and Christopher C. Cummins[a,*]

[a] *Department of Chemistry, Massachusetts Institute of Technology, Cambridge MA, USA;* * *ccummins@mit.edu*

[b] *Max-Planck-Institut für Kohlenforschung, Kaiser-Wilhelm-Platz 1, 45470 Mülheim an der Ruhr, Germany*

Keywords: Azide – Phosphorus – Small Molecule Activation – Thermolysis – Transition Metal Chemistry

Abstract. Phosphorus mononitride (PN) only has a fleeting existence on Earth and molecular precursors for a mild release of the molecule to enable chemical synthesis in solution do not exist. Here we report the synthesis of an anthracene (**A**) based molecular precursor (N_3P**A**) that dissociates into dinitrogen (N_2), **A** and PN in solution with a first order half-life of roughly $t_{1/2} = 30$ min at room temperature associated with an activation enthalpy of $\Delta H^{\ddagger} = 19.5 \pm 1.7$ kcal mol^{-1} and an activation entropy of $\Delta S^{\ddagger} = -8.8 \pm 0.8$ cal mol^{-1} K^{-1}. Heated under vacuum N_3P**A** decomposes in an explosive fashion at around 42 °C as demonstrated in a molecular beam mass spectrometry (MBMS) study. N_3P**A** serves as a PN transfer reagent as demonstrated in the synthesis [(dppe)Fe(Cp*)(NP)][$BArF_{24}$]. Surprisingly, the terminal N-bonded linkage isomer is energetically preferred due to significant covalent iron pnictogen bond character and associated less unfavorable Pauli repulsion in the metal-ligand interaction.

The dinitrogen analogue phosphorus mononitride is the first phosphorus containing compound detected in the interstellar medium in 1987.[1, 2] On Earth, PN was first accidentally prepared in a discharge through air in a tube, which previously had been used with phosphorus by Herzberg *et al.* in 1933 and spectroscopically characterized based on 24 rotational bands.[3] Previously Moldenhauer already reported the formation of a remarkably stable yellow powder in a discharge through nitrogen and phosphorus with a stoichiometry of equal amounts of phosphorus and nitrogen.[4] Alternatively, monomeric PN is formed in the high-vacuum flash pyrolysis of P_3N_5 at 800–900 °C, isolated in solid krypton at 10 K, and characterized based on its single infrared fundamental at 1323 cm^{-1}.[5] In the absence of a noble gas matrix PN polymerizes to $[PN]_n$ and aromatic cyclotriphosphazene $(PN)_3$, which also forms in electron irradiation experiments of ammonia (NH_3) and phosphine (PH_3) containing ices[6] at cryogenic temperatures.[7] The cyclotriphosphazene molecule undergoes a photochemically induced rearrangement to its Dewar benzene-type valence isomer. Under matrix isolation conditions PN was reported to interact with different metal atoms, including Cu, Ag, Au, Co, Ni and Pd.[8] *Ab initio* computations indicate that PN is thermodynamically unstable and formation of N_2 and

diphosphorus (P_2) is exergonic.[9] Klapötke *et al.* described with P_3N_{21} the smallest structurally characterized discrete binary PN molecule so far.[10]

The stabilization and activation of dipnictogens, e.g., N_2,[11] P_2,[12, 13] and just recently PN[14] is still an ongoing endeavor in inorganic chemistry. Due to its high reactivity and the absence of a suitable molecular precursor for a mild release of PN, molecules containing embedded phosphorus mononitride units have been synthesized and stabilized in various fashions, e.g., N-heterocyclic carbenes,[15] anthracene (**A**PN**A**),[16] or cyclo-tetraphosphazene.[17] Niecke and co-workers reported with iminophosphenium tetrachloroaluminate (**1**, Figure 1 top left) the first stable compound with a PN triple bond of 1.475(8) Å according to a crystallographic study.[18] The Bertrand group reported the stabilization of PN by two N-heterocyclic carbenes (**2**, Figure 1 top middle).[15] However, the central P–N interatomic distance was reported in the crystal structure as 1.709(2) Å, which is significantly longer than the triple bond in the gaseous PN molecule determined by microwave spectroscopy to be 1.49086(2) Å.[19] Hence, a better description for the compound would be R'R''C=P–N=CR_2 instead of R'R''C→P≡N←CR_2.[20, 21] A similar result was observed by doubly anthracene stabilized PN in **A**PN**P** (Figure 1 top right).[16] However, from none of these PN-containing complexes could free molecular PN be released, yet. Even the isolation of metal complexes with a PN ligand seems to be challenging because of rapid oligomerization reactions as demonstrated by the phosphinidene reactivity of the transient PNV(N[^{t}Bu]Ar)$_3$ (Ar = 3,5-$Me_2C_6H_3$) complex.[22] Only just recently, Martinez *et al.* reported the synthesis of the first crystallographically characterized PN transition metal complex, namely $[(N_3N)Mo–P{\equiv}N]^-$ (**[Mo](PN)**$^-$), N_3N = $[(Me_3SiNCH_2CH_2)_3N]^{3-}$, which undergoes light-induced linkage isomerization to provide $[(N_3N)Mo–N{\equiv}P]^-$ (**[Mo](NP)**$^-$), as revealed by photocrystallography (Figure 1, bottom).[14] The mononuclear PN complex was released in a reaction of ^{t}BuNC with a bridging PN heterodinuclear complex that was initially synthesized in a reductive coupling of iron(IV) nitride and molybdenum(VI) phosphide complexes.[14]

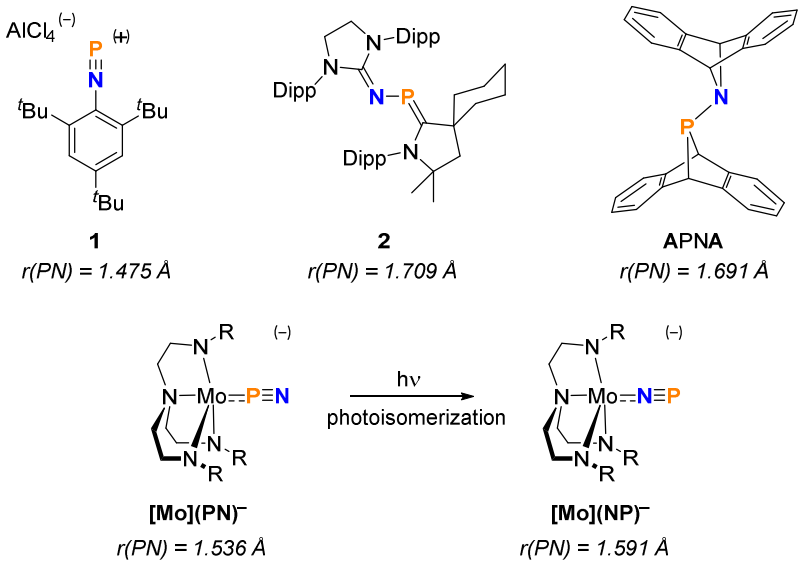

Figure 1 | Selected PN containing molecules and transition metal complexes with given PN bond distances. Top: Iminophosphenium tetrachloroaluminate (**1**, left) as the first stable compound with a PN triple bond (1.475(8) Å). Phosphorus mononitride trapped between two N-heterocyclic carbenes (**2**, middle) and two molecules of anthracene (**A**PN**A**, right) with PN bond distances of 1.709(2) Å and 1.691(1) Å, respectively. Bottom: Anionic molybdenum complex with a PN ligand that isomerizes by irradiation with white light; The PN bond lengths (1.5363(1) Å (left) and 1.5913(1) Å (right)) are only slightly longer than in free PN in the gas-phase (1.49086(2) Å).

Here we report the synthesis of an anthracene based molecular precursor for the release of molecular PN under standard laboratory conditions. In the past dibenzo-7λ^3-phosphanorbornadiene derivatives have already served as suitable precursors for the release of small phosphorus bearing molecules with only anthracene as a leaving group and byproduct.[16, 23-26] According to the literature chlorophosphine Cl**PA**[23] was synthesized and stirred with an excess of sodium azide (NaN_3, 5 equiv.) in tetrahydrofuran (THF) at –20 °C. The addition of lithium chloride (LiCl, 2 equiv.) as a phase-transfer catalyst[27] to solubilize azide ions through conversion of insoluble NaN_3 into soluble LiN_3 and NaCl proved to be highly efficient in reducing the reaction time to 7–10 days and a crude yield of azidophosphine N_3P**A** as a colorless solid of up to 70% after workup (Scheme 2, Figure S1-S3). Single crystals of N_3P**A** grown from diethyl ether at –20 °C were characterized in a single crystal X-ray diffraction experiment and the molecular structure is depicted in Figure 2A (see also Table S3). The structure is in line with a strong infrared band for the azide functional group at 2042 cm^{-1} (Figure S6) and a single signal in the proton decoupled $^{31}P\{^1H\}$ NMR spectrum at δ 180.6 ppm (Figure S2) that is split into a triplet in the proton coupled ^{31}P NMR spectrum with a coupling constant to the two bridgehead protons of anthracene of $^2J_{PH}$ = 14.5 Hz. Isotopically ^{15}N labeled N_3P**A**, was synthesized from sodium azide-1-^{15}N following the same procedure. We obtained a statistical mixture with the ^{15}N isotope bonded to phosphorus as well as at the terminal end of the azide unit. Due to ^{31}P-^{15}N coupling the signal in the $^{31}P\{^1H\}$ NMR is split into a doublet that overlaps with the singlet for the terminal ^{15}N labeled N_3P**A** (Figure S4). The singlet is not exactly in the center of the doublet because of the isotopic shift.[28, 29] We observed two singlet signals at δ 310 and δ 197 ppm in the ^{15}N NMR for both isotopologues that, however, did not split into doublets (Figure S5).

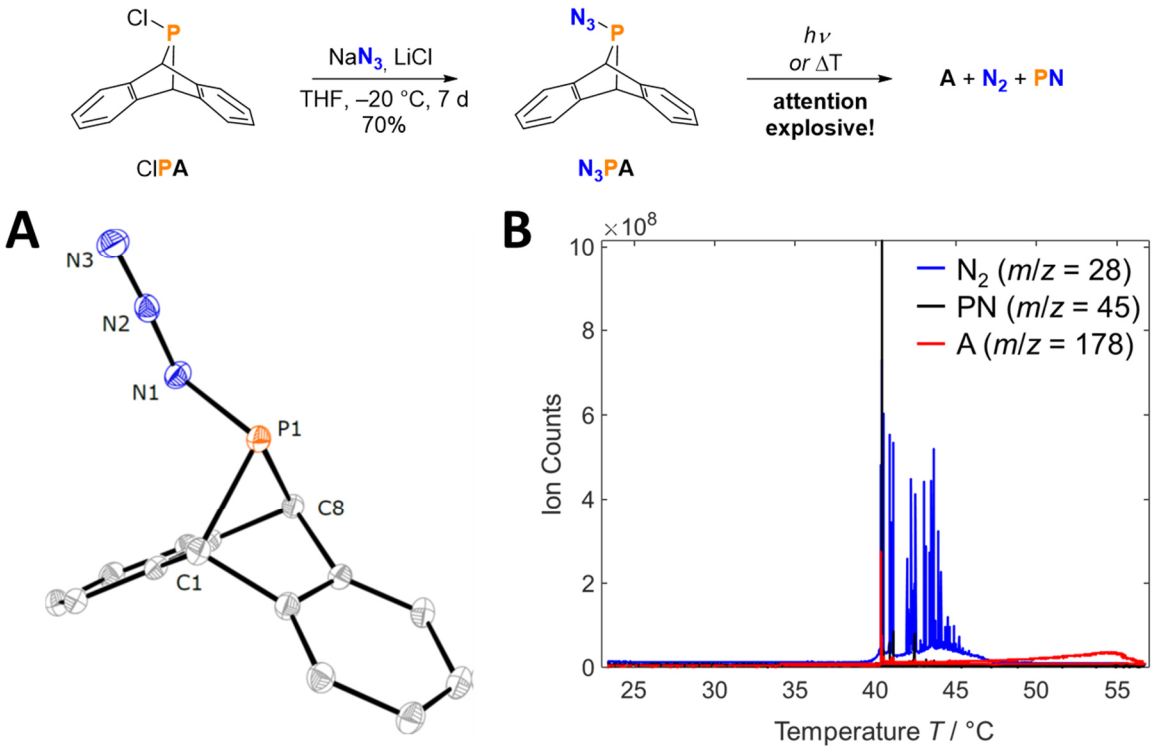

Figure 2 | Synthesis, structure and decomposition of N_3PA. Top: Synthesis of N_3P**A** by nucleophilic substitution of Cl**PA** with NaN_3, catalysed by LiCl in THF at –20 °C. A: Molecular structure of N_3P**A** with thermal ellipsoids shown at the 50% probability level. Hydrogen atoms are omitted for the sake of clarity. Selected interatomic distances (Å): P1−N1 1.7643(14); P1−C1, 1.9025(16); P1−C8, 1.8882(15); N1−N2, 1.2341(18); and

N2−N3, 1.1325(19). Selected interatomic bond angles (°): C1−P1−C8, 80.15(7); P1–N1–N2, 115.22(11). B: Explosive decomposition of N_3P**A** followed by molecular beam mass spectrometry (MBMS).

A melting point of N_3P**A** could not be determined because an explosion occurred at 68 °C. This is in line with the results of our molecular-beam mass spectrometer (MBMS) experiment (Figure 2B); N_3P**A** was heated under vacuum and the released molecules analyzed by mass spectrometry. We observed a strong increase in signals for PN (m/z = 45), N_2 (m/z = 28) and **A** (m/z = 178 and smaller fragments) already at around 42 °C in the chromatogram as a single strong peak that is clear evidence for an explosive decomposition. Gaseous PN is reported to polymerize very easily and form white powder coatings on surfaces and spectroscopic windows.[30] We assume that the polymerization process might also contribute significantly to the observed explosion in our melting point determination. The surface of the sealed capillary was also covered with a white powder coating after the explosion occurred. Phosphorus triazide ($P(N_3)_3$) was reported to decompose smoothly in solution at room temperature with liberation of nitrogen, accompanied by the appearance of a strong ^{31}P resonance at δ 16.2 ppm and a weaker one at δ 6.2 ppm.[31, 32] However, these two signals were not assigned at all but an assignment to the free PN molecule could be excluded. Similar to many other reported P(III) azides, N_3P**A** decomposes smoothly in solution at room temperature under standard conditions.[33] Consequently, we followed the decay of N_3P**A** in benzene-d_6 by ^{1}H NMR spectroscopy (Figure S21-S23, Table S1-S2). The azide decomposes at 25.0 °C with a first order kinetics half-life of around half an hour ($t_{1/2}$ = 29.1 ± 1.6 min) and no new resonances appear in the ^{31}P NMR spectrum. Instead we observed the formation of yellow-orange-brown material in our NMR tube that is line with previously reported PN polymerization products; note that the color of the polymer changes depending on the nitrogen content.[4, 34] Further kinetic measurements on N_3P**A** decomposition were performed over the temperature range of 25–55 °C. An Eyring analysis revealed activation parameters of $\Delta H^{\ddagger}$ = 19.5 ± 1.7 kcal mol^{-1} and $\Delta S^{\ddagger}$ = −8.8 ± 0.8 cal mol^{-1} K^{-1} (Figure S24). The first-order behavior is indicative of a unimolecular rate-determining step, consistent with fragmentation of N_3P**A** into N_2, PN and **A**.

We computed the most essential part of the potential energy surface around N_3P**A** at PBE0-D3(BJ)/cc-pVTZ + Gibbs free energy correction with augmented DLPNO-CCSD(T)/cc-pVTZ single point energies (Figure 3). We located two minima for N_3P**A**, and the energetically preferred conformer is in line with our crystal structure depicted in Figure 2A. In the higher energy conformer the P–N single bond is rotated by 180° and the azide group takes a parallel position to a terminal aromatic ring that results in an energy rise of 0.9 kcal mol^{-1}. Both conformers are connected by a low lying transition state **TS3** (2.9 kcal mol^{-1}). For the decomposition of N_3P**A**, two fragmentation pathways have been considered, first: cleavage of dinitrogen from the azide group and the formation of phosphinonitrene[35] NP**A** (**TS4** 23.3 kcal mol^{-1} and **TS5** 39.8 kcal mol^{-1}) that easily further dissociates into N_2, PN and **A** via **TS6** (1.7 kcal mol^{-1}). The second pathway is connected with the cleavage of anthracene. In an initial step a phosphirane intermediate (**I1**) forms *via* **TS2** (33.9 kcal mol^{-1}) that further dissociates into N_2, PN and **A** via **TS1** (42.5 kcal mol^{-1}). Based on the computed free energy values the first pathway with an initial cleavage of dinitrogen is energetically favored. The minimum energy decomposition pathway with a total barrier of 23.3 kcal mol^{-1} is within the experimental error of our Eyring analysis ($\Delta G^{\ddagger} = \Delta H^{\ddagger} - T\Delta S^{\ddagger}$ = 22.1 ± 1.5 kcal mol^{-1} at 298.15 K).

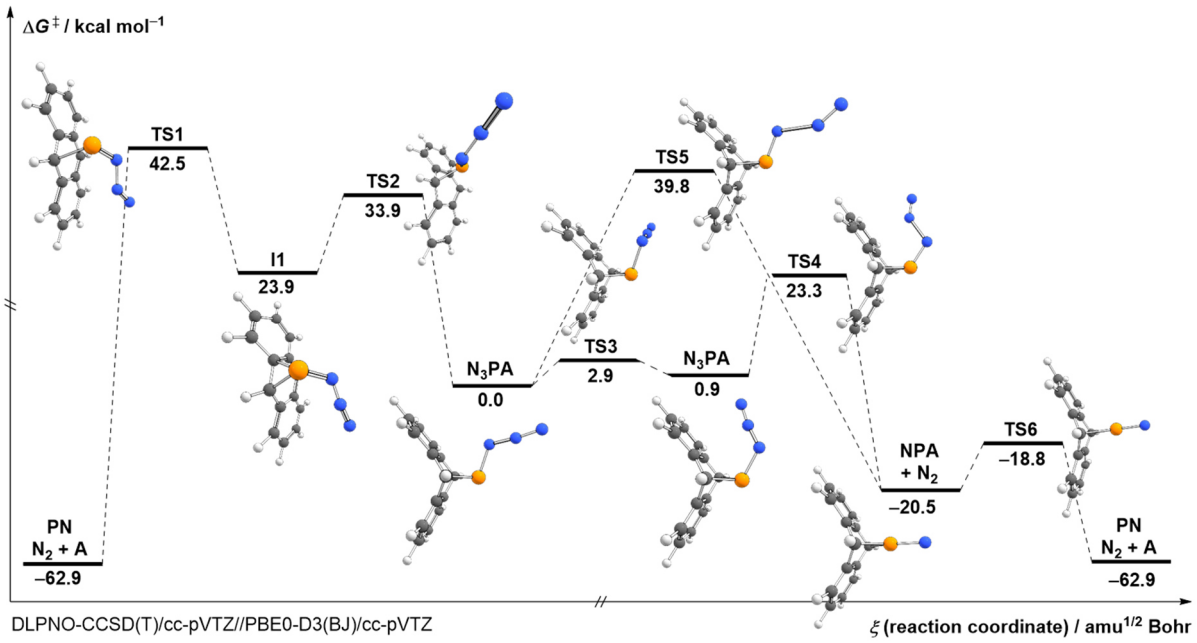

Figure 3 | Computed decomposition pathways of N_3PA. N_3P**A** decomposes into N_2, PN and anthracene either by dinitrogen and subsequent anthracene loss or via a rearrangement to a phosphirane intermediate (**I1**) and subsequent concerted dissociation into N_2, PN and anthracene. Gibbs free energy values are computed for T = 298.15 K. Color code: carbon = grey, hydrogen = white, nitrogen = blue, phosphorus = orange.

Next we focused on the ability of N_3P**A** to transfer a PN molecule as a ligand to a transition metal complex. As indicated by our computations (*vide supra*) the N_3P**A** molecule has two reactive sites. The reaction may be initiated by cleavage of the azide unit in a Staudinger-type reaction[36] with dinitrogen release and the remaining NP**A** unit might be transferred to a transition metal. On the other hand the Cummins group has already demonstrated phosphinidene transfer reactivity of various RP**A** compounds (including R = Me_2N, Et_2N, Me_2Pip, $^iPr_2N$).[37] Inspired by the recent work of Hamon *et al.*[38] we synthesized [(dppe)Fe(Cp*)(N_2)][$BArF_{24}$] (**FeN$_2$**, dppe = 1,2-bis(diphenylphosphino)ethane, Cp* = 1,2,3,4,5-pentamethylcyclopentadienyl, $BArF_{24}$ = Tetrakis[3,5-bis(trifluoromethyl)phenyl]borate) by treatment of (dppe)Fe(Cp*)(Cl) with $NaBArF_{24}$. After stirring the latter two reagents for 60 min in diethyl ether, the initially dark brown solution turned red and a colorless precipitate (NaCl) developed. After filtration through Celite and layering the filtrate with pentane, dark red crystalline blocks formed after one day (Figure S12). **FeN$_2$** was characterized by IR, NMR, and Mößbauer spectroscopy as well as single crystal X-ray crystallography (*vide infra*, Figure 4A, S7-S11, S25 and Table S4). We found a nitrogen-nitrogen bond length of 1.131(7) Å within the single crystal that is only slightly longer than the dinitrogen triple bond in the gas phase (1.09768(5) Å).[39]

Treatment of **FeN$_2$** with an excess of N_3P**A** (~3 equiv.) at room temperature in diethyl ether immediately led to a gas evolution and precipitation of anthracene as a colorless solid. After filtration the filtrate was placed in the freezer to crystallize further **A** that was removed by filtration. The filtrate was layered with pentane. After one day at room temperature dark red crystalline blocks (Figure S20) were observed that were analyzed by IR, NMR, and Mößbauer spectroscopy as well as single crystal X-ray crystallography (*vide infra*, Figure 4B, S13-S17, S26 and Table S5). Our X-ray crystallographic study revealed the successful formation of [(dppe)Fe(Cp*)(NP)][$BArF_{24}$] (**FeNP**) with the previously weak N_2 ligand replaced by PN (Figure 4B). Surprisingly, the PN ligand is terminally N-bonded to the iron center and displays

a PN bond length of 1.493(2) Å that is only slightly longer than in free gaseous PN (1.49086(2) Å, *vide supra*). This is indicative of a weak interaction between the ligand and the metal as also demonstrated in our theoretical analysis (*vide infra*). Intrinsic bond orbital (IBO)[40] analysis reveals a Wiberg bond order of 2.51 for the PN ligand, which is minimally perturbed vis-a-vis the free PN molecule. The P-N bond distance in **FeNP** is longer than in in crystalline $[Mes^*NP]^+$ salts (Mes* = 2,4,6-^{t}Bu$_3$C$_6$H$_2$), e.g., 1.475(8) Å in **1** or 1.467(4) in [Mes*NP][OTf] (OTf = $CF_3SO_3^-$).[18, 41] In comparison to **[Mo](PN)**$^-$ the PN distance is approximately 0.043 Å shorter.[14] The Wiberg bond order for PN in **[Mo](PN)**$^-$ is 2.13. IBO charges reveal an almost neutral PN ligand in **FeNP** (N: –0.57, P: 0.57) in stark contrast to **[Mo](PN)**$^-$ where the PN ligand carries an overall significant negative charge (N: –0.95, P: 0.57). This is consistent with the latter system having considerably more back-bonding to the PN ligand (*c.f.* Figure 5 and S31).

The diamagnetic nature of the two prepared transition metal complexes allowed us further spectroscopic characterization by multinuclear NMR spectroscopy. The singlet signal at δ 85 ppm in the $^{31}P\{^1H\}$ spectrum of the dppe ligand in **FeN$_2$** (Figure 4C left, S9) is split into a doublet in **FeNP** and slightly shifted downfield to δ 86 ppm (Figure 4C right, S15). In addition, a triplet resonance is observed for the NP ligand at δ 271 ppm with a coupling constant of $^3J_{PP}$ = 9.2 Hz. We synthesized 50% enriched **Fe$^{14/15}$NP** by treatment of **FeN$_2$** with ^{15}N labeled **^{15}N$_3$PA** (*vide supra*). In the ~50% ^{15}N isotopically enriched **Fe$^{14/15}$NP** complex the triplet resonance at at δ 271 ppm splits into a doublet of triplets, partially overlapping with the unlabeled triplet (Figure S18). A weak doublet at δ 450 pm ($^1J_{NP}$ = 51.1 Hz) is observed in the ^{15}N NMR spectrum (Figure S19). Our attempts to determine the ^{31}P-^{57}Fe coupling constant between the PN ligand and the iron center failed. We were only able to determine the coupling constant of the dppe ligand to the ^{57}Fe center to be $^1J_{FeP}$ = 55.4 Hz in **FeN$_2$** (Figure S11) and $^1J_{FeP}$ = 56.5 Hz in **FeNP** (Figure S17).

We collected solid-state infrared (IR) data of all three crystallized complexes (Figure 4C middle) and observed a strong sharp band at 2116.3 cm^{-1} in **FeN$_2$** that is characteristic for a ν_{NN} stretching vibration. The band is not present for the **FeNP** complex. The high wavenumber of 2116.3 cm^{-1} in comparison to other transition metal dinitrogen complexes is indicative for a weak Fe–N bond.[42] For **FeNP** we observed a shoulder signal at 1270.7 cm^{-1} that is overlapping with another signal but clearly not present in **FeN$_2$**. We assign this signal to the ν_{NP} stretching mode that is red shifted by roughly $\Delta\nu$ = 52 cm^{-1} in comparison to free PN (ν_{NP} = 1323 cm^{-1}).[5, 30] A new band appeared for isotopically labeled **Fe^{15}NP** at 1238.3 cm^{-1}. The experimental isotope shift for the ν_{NP} stretching vibration is $\Delta\nu_{exp}$ = 32.4 cm^{-1} that is in good agreement with a computed harmonic shift of $\Delta\nu_{calc}$ = 34.6 cm^{-1} at the PBE0-D3(BJ)/cc-pVTZ level of theory.

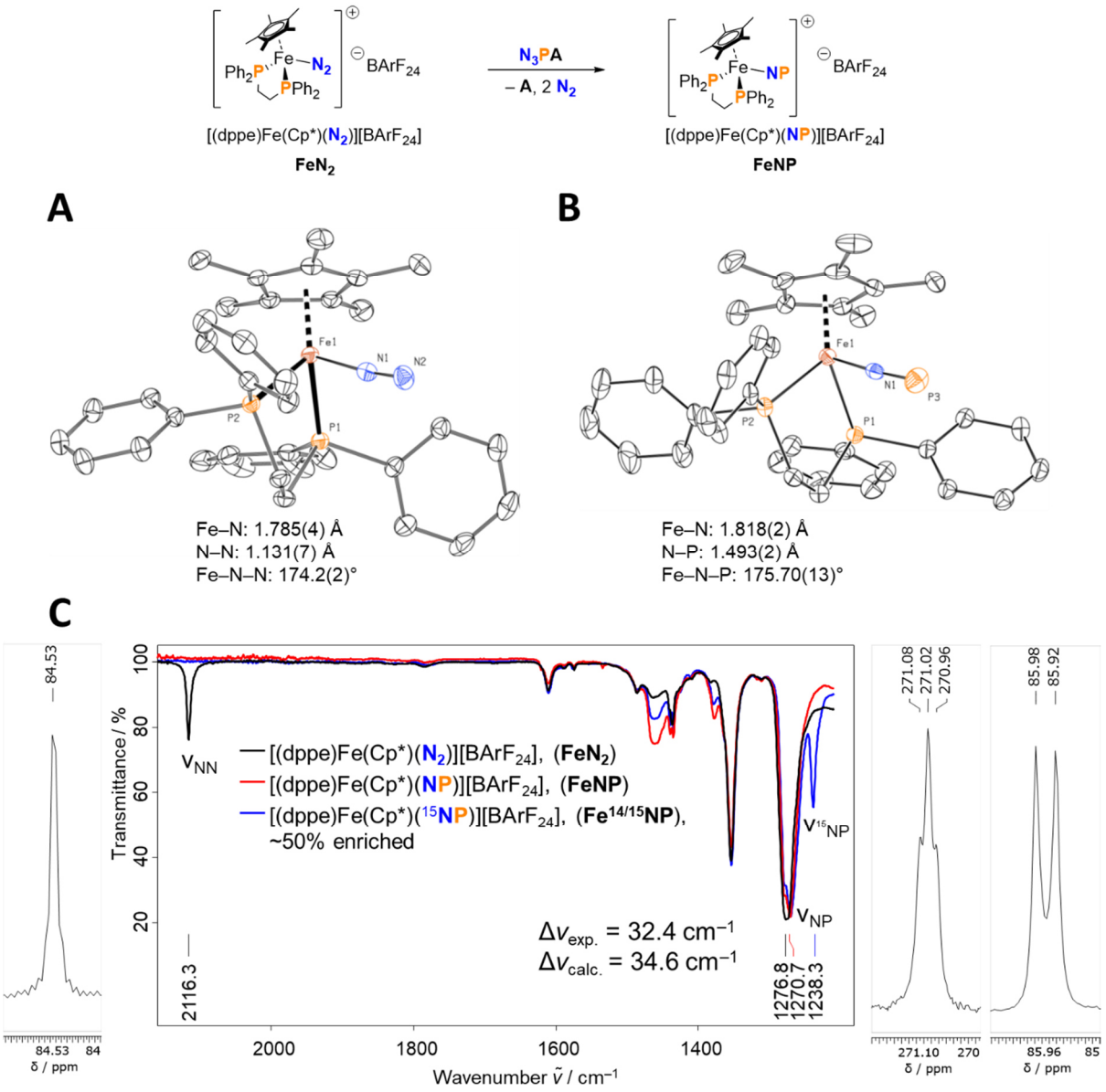

Figure 4 | Synthesis, structure and spectroscopic characterization of FeN_2 and FeNP. Top: Synthesis of **FeNP**. **A**: Molecular structure of FeN_2 with thermal ellipsoids shown at the 50% probability level. Hydrogen atoms are omitted for the sake of clarity. **B**: Molecular structure of **FeNP** with thermal ellipsoids shown at the 50% probability level. Hydrogen atoms are omitted for the sake of clarity. **C:** Middle: Infrared spectrum of FeN_2 (black), **FeNP** (red) and $Fe^{14/15}NP$ (blue, ~50% enriched with ^{15}N); left and right $^{31}P\{^1H\}$ NMR spectrum of FeN_2 and **FeNP**, respectively.

We recorded ^{57}Fe Mößbauer spectra of FeN_2 and **FeNP** at 80 K and fitted the data with two Lorentzian functions as included in the WMOSS software (Figure S25 and S26).[43] The spectra of the two complexes show a single doublet which clearly establishes the spectroscopic purity of the samples in line with our other analytical characterization methods (see elemental analysis in Methods section). The line broadening of both complexes ($\Gamma = 0.266$ mm s^{-1} for FeN_2 and $\Gamma = 0.269$ mm s^{-1} for **FeNP**) is similar to the previously reported [(dppe)Fe(Cp*)][PF_6] complex ($\Gamma = 0.257$ mm s^{-1}).[38] The isomer shift (δ) for FeN_2 is $\delta = 0.395$ mm s^{-1} and for **FeNP** is $\delta = 0.299$ mm s^{-1}. The quadrupole splitting (ΔE_Q) for FeN_2 is $\Delta E_Q = 2.018$ mm s^{-1} and for **FeNP** is $\Delta E_Q = 1.696$ mm s^{-1}. The experimental values are in good agreement with our calculations of the corresponding cations; $\delta = 0.409$ mm s^{-1} and $\Delta E_Q = 2.008$ mm s^{-1} for FeN_2^+ and $\delta = 0.317$ mm s^{-1} and $\Delta E_Q = 1.712$ mm s^{-1} for $FeNP^+$ (see SI for further details). The

experimental difference of roughly 0.1 mm s^{-1} for the isomer shift is a hint for a greater covalency in **FeNP**. Similar observations have been reported by the Peters group. In the [K(benzo-15-crown-2)$_2$][((Ph$_2$PCH$_2$SiMe$_2$)$_3$CH)Fe(L)] system the isomer shift for L = CO is 0.18 mm s^{-1} lower than that for L = N_2, consistent with stronger CO π backbonding.[44] Our computed reduced Mulliken (**FeN$_2$$^+$**: 0.84, **FeNP$^+$**: 0.94) and Löwdin (**FeN$_2$$^+$**: 0.88, **FeNP$^+$**: 0.97) orbital charges show a significant higher charge for the Fe d_{yz} orbital for the **FeNP$^+$** system. The higher orbital charge is related with the experimentally observed lower isomer shift and stronger π backbonding in **FeNP** (*vide infra*).

We explored the potential energy surface around **FeNP** computationally. As a global energetic minimum we located a closed shell (S = 0, with S as the total spin number of the system) low spin electronic ground state for the [(dppe)Fe(Cp*)(NP)]$^+$ cation (**FeNP$^+$**) at the DLPNO-CCSD(T)/cc-pVTZ//PBE0-D3(BJ)/cc-pVTZ + thermal correction to Gibbs free energy level of theory (Figure 5). Isomerization of the NP ligand occurs via the side-on bound isomer that is connected via **TS1** (25.5 kcal mol^{-1}, Figure 5) to **FeNP$^+$** and 16.8 kcal mol^{-1} energetically less preferred. Further isomerization via **TS2** (36.6 kcal mol^{-1}, Figure 5) leads to the PN linkage isomer **FePN$^+$** that is surprisingly 14.3 kcal mol^{-1} higher in energy than the **FeNP$^+$** isomer. We computed the ^{31}P NMR chemical shifts of all three isomers according to a literature benchmark study at the PBE0-D3(BJ)/6-31G(d) level of theory.[45] According to the computations all three isomers should be distinguishable by NMR spectroscopy as they are separated by roughly 80 ppm (Figure 5). The computed chemical shift for **FeNP$^+$** with δ 282 ppm is in good agreement with the experimentally observed resonance at δ 271 ppm. The energetic high barrier of **TS2** (36.6 kcal mol^{-1}) prevents isomerization of the NP ligand at room temperature. Even after refluxing the complex in toluene or after irradiation with green and yellow light with light emitting diodes (LEDs) we did not observe any new resonance by ^{31}P NMR spectroscopy.

The energetic preference of the **FeNP$^+$** isomer vs the **FePN$^+$** is surprising because we initially expected a better orbital overlap between iron and phosphorus and a preference of the **FePN$^+$** isomer. However, our local energy decomposition (LED)[46] and natural orbital chemical valence (NOVC)[47] analysis indicates that the interaction between the ligand and the metal center is of significant covalent nature (see Figure 5 top for intrinsic bond orbitals (IBOs) and Figure S27-S30 and Table S6-S11). In the NOCV/EDA analysis[48] of **FeNP$^+$** we obtain an energy of –90.8 kcal mol^{-1} (Table S5) for the orbital interaction term ΔE_{orb}, representing orbital mixing effects, *e.g.*, charge transfer and polarization effects. As the term is similar for **FePN$^+$** (–98.8 kcal mol^{-1}), this is indicative that the interaction between the ligand and the metal center is strongly covalent in nature and mainly dominated by the ΔE_{steric} term (44.0 kcal mol^{-1} for **FeNP$^+$** and 66.8 kcal mol^{-1} for **FePN$^+$**). The most important mixing contributions for **FeNP$^+$** is the π-backdonation from the occupied d orbitals of suitable symmetry on the Fe atom to the empty LUMO antibonding π^* orbitals of the ligand $\Delta E_{orb}[d(\text{Fe}) \rightarrow \pi^*(\text{NP})]$ (–28.6 kcal mol^{-1}, Figure S31) and $\Delta E_{orb}[d(\text{Fe}) \rightarrow \pi_\perp(\text{NP})]$ (–21.9 kcal mol^{-1}, Figure S31). Another significant contribution is the σ-donation from the HOMO of the ligand to the empty d orbitals of Fe $\Delta E_{orb}[\sigma(\text{NP}) \rightarrow d(\text{Fe})]$ (–32.1 kcal mol^{-1}, Figure S31). The relative stability of the isomers correlates well only with Pauli repulsion effects. Thus, the relative stability between the isomers essentially originates from the fact that the atomic orbitals on phosphorus are larger and more diffuse than those on nitrogen. This causes an increase in Pauli repulsion when the ligand coordinates from the phosphorus side. This is not compensated by a corresponding increase in orbital interactions, as quantified by the NOCV scheme (Table S11). With a

dinitrogen ligand in **FeN$_2$$^+$** the orbital interactions are qualitatively the same as in **FeNP$^+$**. In general, the frontier orbitals of N_2 are of similar shape and nature as in PN (Figure S30). However, the LUMO orbitals of N_2 feature higher energies than those of PN, whilst the HOMO and HOMO–1 orbitals show lower energies. Hence, N_2 is expected to be a poorer π acceptor as well as a poorer σ donor than PN. This is confirmed by our NOCV/EDA analysis. All donation and back donation components are smaller in **FeN$_2$$^+$** ($\Delta E_{orb}[d(Fe) \rightarrow \pi^*(N_2)] = -22.2$ kcal mol^{-1}; $\Delta E_{orb}[d(Fe) \rightarrow \pi_\perp(N_2)] = -18.1$ kcal mol^{-1} and $\Delta E_{orb}[\sigma(N_2) \rightarrow d(Fe)]$ (–24.1.1 kcal mol^{-1}) than in **FeNP$^+$** (Table S11). The covalent interaction between the iron center and the PN ligand is also shown by IBO analysis (Figure 5 top). The backbonding of the metal to the ligand is only minimal (see second row right orbital in Figure 5) and in stark contrast to the situation for **[Mo](PN)$^-$** complex reported by the Smith group (Figure S31).

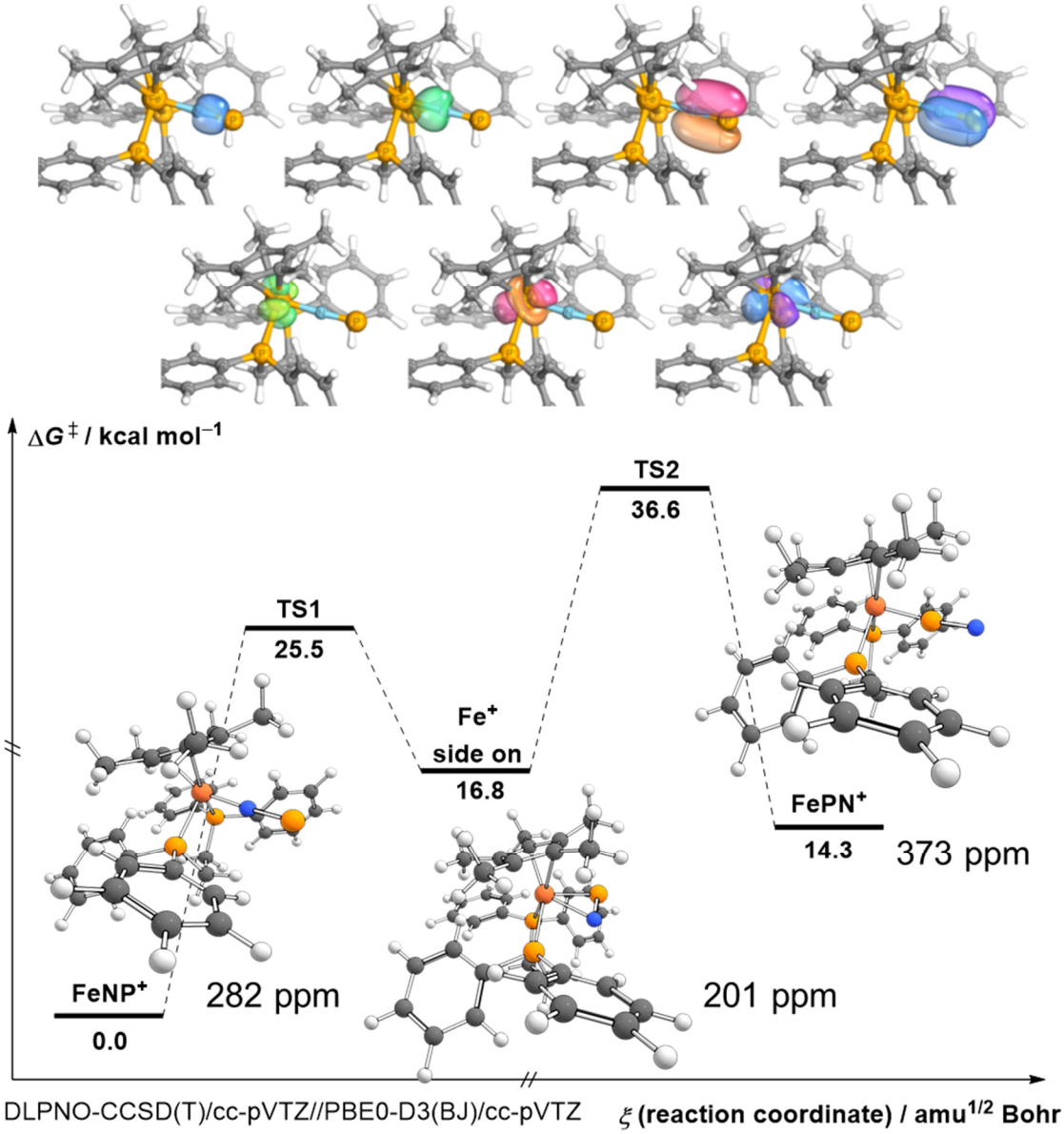

Figure 5 | Isomerization of the PN ligand in [(dppe)Fe(Cp*)(NP)]$^+$ and analysis of the bonding situation. Top: Selected intrinsic bond orbitals (IBOs): The top row shows the σ_{PN}, the σ_{FeN}, and the two π_{PN} bonds. The bottom row shows the three doubly occupied *d* orbitals of this d^6 complex. Bottom: Potential energy surface for the isomerization of the PN ligand. Color code: carbon = grey, hydrogen = white, nitrogen = blue, phosphorus = orange, iron = brown.

In summary, we presented the synthesis and development of a molecular precursor $N_3P\mathbf{A}$ that dissociates at room temperature and slowly releases dinitrogen, anthracene and phosphorus mononitride with a half-life of roughly half an hour. Phosphorus mononitride polymerizes very rapidly in solution by forming yellow-orange-brown polymers but can be efficiently transferred and trapped as demonstrated by the synthesis of [(dppe)Fe(Cp*)(NP)][$BArF_{24}$]. The PN ligand is surprisingly N-bonded to the iron center because of a significant covalent iron pnictogen bond character that results in less Pauli repulsion when the ligand coordinates from the N side. The synthesis of $N_3P\mathbf{A}$ and the prepared iron complex with a PN ligand opens new pathways to conduct further reactivity studies of the PN molecule in the future.

Methods

Caution. The handling of azide compounds should be done with the necessary safety precautions.[49] No direct explosions of $N_3P\mathbf{A}$ were encountered when it was diluted in organic solvents or carefully dried under vacuum below room temperature. Treatment of transition metal complexes in solution with solid $N_3P\mathbf{A}$ can cause a spontaneous explosive decomposition of $N_3P\mathbf{A}$ and should be avoided or solid $N_3P\mathbf{A}$ only be added in portions of a few milligrams, respectively.

All manipulations were performed in a Vacuum Atmospheres model MO-40M glovebox under an inert atmosphere of purified N_2. All solvents were obtained anhydrous and oxygen-free by bubble degassing (N_2) and purification through columns of alumina and Q5,[50] and storage over molecular sieves.[51] Literature procedures were followed for the preparation of Mg**A**·3THF,[37] $Me_2NP\mathbf{A}$,[23] Cl$P\mathbf{A}^{\mathbf{23}}$ (**A** = $C_{14}H_{10}$, anthracene) and (dppe)Fe(Cp*)(Cl).[52, 53] Dimethylaminophosphorus dichloride (Me_2NPCl_2) was purchased from Alfa Aesar and used as received. Lithium chloride (LiCl) and sodium azide (NaN_3) were purchased from Sigma Aldrich and used as received. Deuterated solvents were purchased from Cambridge Isotope Laboratories, degassed, and stored over molecular sieves for at least 48 h prior to use. Activated Charcoal Norit CA1 (Aldrich) and Celite 435 (EM Science) were dried by heating above 200 °C under dynamic vacuum for at least 48 h. All glassware was oven dried for at least 3 h at temperatures greater than 150 °C. NMR spectra were obtained on Bruker Avance 400, 401 or Bruker Neo 500 instruments equipped with Magnex Scientific superconducting magnets. ^{1}H and ^{13}C NMR spectra were referenced to residual protiated solvent resonances;[54] ^{31}P NMR spectra were referenced externally to 85% aqueous H_3PO_4 (δ = 0 ppm). Elemental analyses were performed by Midwest Microlab (Indianapolis, IN). High resolution mass spectral (HRMS) data were collected using a Jeol AccuTOF 4G LC-Plus mass spectrometer equipped with an Ion-Sense DART source. Data were calibrated to a sample of PEG-600 and were collected in positive ion mode. Samples were prepared in THF (ca. 10 μM concentration) and were briefly exposed to air (<5 s) before being placed in front of the DART source. Zero-field ^{57}Fe Mößbauer spectra were measured with a constant acceleration spectrometer at 80 K with isomer shifts reported relative to Fe foil at 298 K (0 mm s^{-1}); data were analyzed and simulated with WMOSS v4.[43]

Synthesis of $N_3P\mathbf{A}$. Inside the glovebox, a 20 mL vial was charged with solid, colorless Cl$P\mathbf{A}$ (500 mg, 2.04 mmol, 1.0 equiv.), NaN_3 (675 mg, 10.38 mmol, 5.0 equiv.), LiCl (180 mg, 4.25 mmol, 2.0 equiv.) and a magnetic stir bar. Precooled (–20 °C) THF (15 mL) was added to the vial that was tightly closed with a cap and subsequently transported to the freezer inside the glovebox where it was stirred in the dark for 7 d at –20 °C. After seven days, all volatiles were removed under reduced pressure to yield a cream-colored solid residue. The solids were slurried in diethyl ether (4 x 20 mL) at room temperature and filtered through a celite:charcoal (1:1, 4 cm) plug in a 15 mL medium frit. The colorless ethereal solution was collected in a filter flask that was precooled in the liquid N_2 immersed coldwell of the glovebox. Removal of solvent *in vacuo* from the colorless filtrate left a colorless solid that was weighed and stored in the freezer. Yields varied depending on how much anthracene was produced during the course of the reaction and the workup, giving up to 360 mg (70%) crude product with some anthracene

impurities that rapidly decomposes at room temperature yielding a yellowish mixture of anthracene and PN polymers. The identity of the product was confirmed by NMR and IR spectroscopy as well as by an X-ray diffraction study performed on a crystal grown from diethyl ether at –20 °C (Figure 2A). A melting point for this material could not be determined. At 46.0 ± 0.5 °C the compound decomposes in an explosive fashion. DART HRMS(Q-TOF) *m/z*: $[M + H]^+$ Calcd for $C_{14}H_{11}N_3P$ 252.0685; Found 252.0698. ^{1}H NMR (benzene-d_6, 400 MHz, 25 °C) δ 7.41 (m, 2H), 7.33 (m, 2H), 7.17(m, 2H), 6.98 (m, 2H), 4.06 (d, 2H, $^2J_{PH}$ = 12.6 Hz, H4) ppm. ^{13}C{^{1}H} NMR (benzene-d_6, 126 MHz, 25 °C) δ 145.9 (d, J = 3.1 Hz), 141.7 (d, J = 22.5 Hz), 126.5, 125.2, 124.5, 123.7 (d, J = 3.5 Hz), 56.8 (d, J = 18.9 Hz) ppm. ^{31}P{^{1}H} NMR (benzene-d_6, 162 MHz, 25 °C) δ 181 ppm. X-^{15}N ^{31}P{^{1}H} NMR (benzene-d_6, 162 MHz, 25 °C) δ 181 (d, J_{PN} = 77.9 Hz), 181 (s, b) ppm. ^{15}N NMR (benzene-d_6, 50.7 MHz, 25 °C) δ 310, 197 ppm.

Synthesis of [(dppe)Fe(Cp*)(N$_2$)][BArF$_{24}$]. To a stirring solution of 100 mg (0.159 mmol) (dppe)Fe(Cp*)Cl in diethyl ether (4 mL) was added 141 mg (0.159 mmol, 1 equiv.) NaBArF$_{24}$ portionwise. After stirring for 60 min, the initially dark brown solution became pale red and a precipitate formed. The solution was filtered through Celite and the solvent removed from the filtrate. The red solids were triturated with pentane (3 x 2 mL) and dried under vacuum. The solids were dissolved in 2 mL diethyl ether and layered with 5 mL pentane to crystallize [(dppe)Fe(Cp*)(N$_2$)][BArF$_{24}$]. After 24 h at room temperature large dark red blocks formed out of solution. These blocks were analyzed by NMR spectroscopy and in a X-ray diffraction crystallographic study. Yield: 173 mg (0.116 mmol, 73%). Anal. Calcd for $C_{68}H_{51}BF_{24}FeN_2P_2$: C, 55.16; H, 3.47; N, 4.54. Found: C, 54.76; H, 3.84; N, 0.0. ^{1}H NMR (diethyl ether (solvent suppressed), 500 MHz, 25 °C) δ 8.27 (m, 8H, BArF$_{24}$), 8.10 (m, found 14H, expected 16H), 8.03 (m, 4 H), 7.91 (m, 4H, BArF$_{24}$), 2.96 (m, 2H), 2.81 (m, 2H), 1.92 (s, 15H) ppm. ^{13}C{^{1}H} NMR (diethyl ether, 126 MHz, 25 °C) δ 162.1 (q, J = 50.0 Hz), 135.1 (m), 133.7 (m), 132.6 (m), 13.6 (d, J= 29.6 Hz), 130.9 (m), 129.6 (m), 125.0 (q, J = 272.0 Hz), 117.5 (m), 92.2 , 28.7, 9.0 ppm. ^{31}P{^{1}H} NMR (diethyl ether, solvent suppressed, 203 MHz, 25 °C) 85 ppm. IR (ATR, crystals covered with oil under air): 2117 cm^{-1} (ν_{NN}).

Synthesis of [(dppe)Fe(Cp*)(NP)][BArF$_{24}$]. Inside the glovebox, to a stirring solution of 55 mg (0.037 mmol) [(dppe)Fe(Cp*)(N$_2$)][BArF$_{24}$] in diethyl ether (5 mL) was added carefully 37 mg (0.148 mmol, ~4 equiv.) N$_3$P**A** portionwise. Gas evolution occured immediately and a precipitate (anthracene) develops. The solution was filtered after stirring for 15 min and placed in the freezer for 2 h to crystallize out any further anthracene. After two hours anthracene was filtered off and the resulting solution layered with 5 mL pentane to crystallize [(dppe)Fe(Cp*)(NP)][BArF$_{24}$]. After 24 h at room temperature large dark red blocks formed out of solution. These blocks were analyzed by NMR spectroscopy and in a X-ray diffraction crystallographic study. Yield: 40 mg (0.027 mmol, 73%). Anal. Calcd for $C_{68}H_{51}BF_{24}FeNP_3$: C, 54.53; H, 3.43; N, 0.94. Found: C, 54.20; H, 3.55; N, 0.34. ^{1}H NMR (diethyl ether (solvent suppressed), 400 MHz, 25 °C) δ 8.43 (m, found 9H, expected 8H, BArF$_{24}$), 8.20 (m, 20H), 8.01 (m, 4H, BArF$_{24}$), 3.31 (m, 2H), 3.01 (m, 2 H), 1.98 (s, 15 H) ppm. ^{13}C{^{1}H} NMR (diethyl ether, 126 MHz, 25 °C) δ 162.2 (q, J = 50.0 Hz, BArF$_{24}$), 135.3 (s (b), BArF$_{24}$), 133.8 (m), 133.6 (m), 132.7 (d, J = 29.6 Hz), 129.8 (m, BArF$_{24}$), 129.5 (m), 125.2 (q, J = 272.0 Hz, BArF$_{24}$), 117.7, 94.7, 28.1 (m), 9.0 (d, J = 29.6 Hz ppm. ^{31}P{^{1}H} NMR (diethyl ether, solvent suppressed, 203 MHz, 25 °C) 271 (t, J = 9.2), 86 (d, J = 8.8) ppm. ^{15}N enriched sample: ^{31}P{^{1}H} NMR (diethyl ether, solvent suppressed, 203 MHz, 25 °C) 271 (dt, J_{PN} = 53.4, J_{PP} = 9.5), 86 (d, J_{PP} = 8.5) ppm. ^{15}N NMR (diethyl ether, solvent suppressed, 50.7 MHz, 25 °C) δ 450 (d, J_{PN} = 51.1) ppm.

Data Availability

All relevant data generated and analyzed during this study, including crystal structures, NMR, IR, MBMS spectra and optimized coordinates for all calculated compounds, are included in this Article and its Supplementary Information, and are also available from the authors upon reasonable request.

Acknowledgements

A.K.E. thanks the Alexander von Humboldt foundation for a Feodor Lynen postdoctoral fellowship. This material is based on research supported by the National Science Foundation, under No. CHE-1955612. We thank all MIT DCIF staff members and Dr. Clemens Anklin (Bruker) for technical support with NMR measurements, as well as Michael C. McCarthy (Harvard CfA), Robert J. Gilliard (University of Virginia) and Daniel L.M. Suess (MIT) for fruitful discussion.

Author contributions

A.K.E. conducted all experiments, carried out the computations of the potential energy surfaces and analyzed the data. M.-L.Y.R. and P.M. collected all diffraction data and refined the structures. M.Y. collected all Mößbauer data. G.B. analyzed the bonding situation in [(dppe)Fe(Cp*)(NP)][$BArF_{24}$]. C.C.C. administrated the study. A.K.E. wrote the manuscript with input from all authors.

Competing financial interests

None.

Materials & Correspondence

Correspondence and material requests should be addressed to C.C.C.

Orcid

A.K.E. 0000-0003-1029-9272
M.L.Y.R. 0000-0002-0900-3545
M.Y. 0000-0003-2709-8135
P.M. 0000-0001-6530-3852
G.B. 0000-0003-4849-1323
C.C.C. 0000-0003-2568-3269

References

1. Ziurys L. Detection of interstellar PN-the first phosphorus-bearing species observed in molecular clouds. *Astrophys. J.* **321**, L81-L85 (1987).

2. Turner B, Bally J. Detection of interstellar PN-The first identified phosphorus compound in the interstellar medium. *Astrophys. J.* **321**, L75-L79 (1987).
3. Curry J, Herzberg L, Herzberg G. Spectroscopic Evidence for the Molecule PN. *J. Chem. Phys.* **1**, 749-749 (1933).
4. Moldenhauer W, Dörsam H. Über die Vereinigung von Phosphor und Stickstoff unter dem Einflusse elektrischer Entladungen. *Ber. dtsch. Chem. Ges. A/B* **59**, 926-931 (1926).
5. Atkins RM, Timms PL. The matrix infrared spectrum of PN and SiS. *Spectrochim. Acta, Part A* **33**, 853-857 (1977).
6. Zhu C, Bergantini A, Singh SK, Kaiser RI, Eckhardt AK, Schreiner PR*, et al.* Formation of phosphine imide ($HN{=}PH_3$) and its phosphinous amide (H_2N-PH_2) isomer. *Chem. Commun.* **57**, 4958-4961 (2021).
7. Zhu C, Eckhardt AK, Bergantini A, Singh SK, Schreiner PR, Kaiser RI. The elusive cyclotriphosphazene molecule and its Dewar benzene–type valence isomer (P_3N_3). *Sci. Adv.* **6**, eaba6934 (2020).
8. Atkins RM, Timms PL. Interaction of PN with metal atoms in a krypton matrix. *Inorg. Nucl. Chem. Letters* **14**, 113-115 (1978).
9. Ahlrichs R, Bär M, Plitt HS, Schnöckel H. The stability of PN and $(PN)_3$. Ab initio calculations and matrix infrared investigations. *Chem. Phys. Lett.* **161**, 179-184 (1989).
10. Göbel M, Karaghiosoff K, Klapötke TM. The First Structural Characterization of a Binary P–N Molecule: The Highly Energetic Compound P_3N_{21}. *Angew. Chem. Int. Ed.* **45**, 6037-6040 (2006).
11. McSkimming A, Suess DLM. Dinitrogen binding and activation at a molybdenum–iron–sulfur cluster. *Nat. Chem.* **13**, 666-670 (2021).
12. Sun J, Verplancke H, Schweizer JI, Diefenbach M, Würtele C, Otte M*, et al.* Stabilizing P≡P: P_2^{2-}, $P_2^{\cdot-}$, and P_2^0 as bridging ligands. *Chem* **7**, 1952-1962 (2021).
13. Du J, Hunger D, Seed JA, Cryer JD, King DM, Wooles AJ*, et al.* Dipnictogen f-Element Chemistry: A Diphosphorus Uranium Complex. *J. Am. Chem. Soc.* **143**, 5343-5348 (2021).
14. Martinez JL, Lutz SA, Beagan DM, Gao X, Pink M, Chen C-H*, et al.* Stabilization of the Dinitrogen Analogue, Phosphorus Nitride. *ACS Cent. Sci.* **6**, 1572-1577 (2020).
15. Kinjo R, Donnadieu B, Bertrand G. Isolation of a Carbene-Stabilized Phosphorus Mononitride and Its Radical Cation (PN+.). *Angew. Chem. Int. Ed.* **49**, 5930-5933 (2010).
16. Velian A, Cummins CC. Facile Synthesis of Dibenzo-7λ^3-phosphanorbornadiene Derivatives Using Magnesium Anthracene. *J. Am. Chem. Soc.* **134**, 13978-13981 (2012).
17. Hering C, Schulz A, Villinger A. Diatomic PN – trapped in a cyclo-tetraphosphazene. *Chem. Sci.* **5**, 1064-1073 (2014).
18. Niecke E, Nieger M, Reichert F. Arylmino(halogeno)phosphanes $XP{=}NC_6H_2tBu_3$ (X = Cl, Br, I) and the Iminophosphenium Tetrachloroaluminate $[P{\equiv}NC6H2tBu3]^+[AlCl4]^-$: the First Stable Compound with a PN Triple Bond. *Angew. Chem. Int. Ed.* **27**, 1715-1716 (1988).
19. Wyse FC, Manson EL, Gordy W. Millimeter Wave Rotational Spectrum and Molecular Constants of $^{31}P^{14}N$. *J. Chem. Phys.* **57**, 1106-1108 (1972).
20. Tofan D, Velian A. Interstellar Chemistry in a Glovebox: Elusive Diatomic P≡N, Exposed. *ACS Cent. Sci.* **6**, 1485-1487 (2020).
21. Himmel D, Krossing I, Schnepf A. Dative Bonds in Main-Group Compounds: A Case for Fewer Arrows! *Angew. Chem. Int. Ed.* **53**, 370-374 (2014).
22. Courtemanche M-A, Transue WJ, Cummins CC. Phosphinidene Reactivity of a Transient Vanadium P≡N Complex. *J. Am. Chem. Soc.* **138**, 16220-16223 (2016).
23. Velian A, Nava M, Temprado M, Zhou Y, Field RW, Cummins CC. A Retro Diels–Alder Route to Diphosphorus Chemistry: Molecular Precursor Synthesis, Kinetics of P_2 Transfer to 1,3-Dienes, and Detection of P_2 by Molecular Beam Mass Spectrometry. *J. Am. Chem. Soc.* **136**, 13586-13589 (2014).
24. Transue WJ, Velian A, Nava M, Martin-Drumel M-A, Womack CC, Jiang J*, et al.* A Molecular Precursor to Phosphaethyne and Its Application in Synthesis of the Aromatic 1,2,3,4-Phosphatriazolate Anion. *J. Am. Chem. Soc.* **138**, 6731-6734 (2016).
25. Transue WJ, Nava M, Terban MW, Yang J, Greenberg MW, Wu G*, et al.* Anthracene as a Launchpad for a Phosphinidene Sulfide and for Generation of a Phosphorus–Sulfur Material

Having the Composition P_2S, a Vulcanized Red Phosphorus That Is Yellow. *J. Am. Chem. Soc.* **141**, 431-440 (2019).
26. Riu M-LY, Jones RL, Transue WJ, Müller P, Cummins CC. Isolation of an elusive phosphatetrahedrane. *Sci. Adv.* **6**, eaaz3168 (2020).
27. Gediga M, Burck S, Bender J, Förster D, Nieger M, Gudat D. Specific and Reversible Alkynyl Transfer Reactions of an N-Heterocyclic Phosphane. *Eur. J. Inorg. Chem.* **2014**, 1818-1825 (2014).
28. Hansen PE. Isotope Effects on Nuclear Shielding. In: Webb GA (ed). *Annual Reports on NMR Spectroscopy*, vol. 15. Academic Press, 1984, pp 105-234.
29. Hansen PE. Isotope effects in nuclear shielding. *Prog. Nucl. Magn. Reson. Spectrosc.* **20**, 207-255 (1988).
30. Ahmad IK, Hamilton PA. The Fourier Transform Infrared Spectrum of PN. *J. Mol. Spectrosc.* **169**, 286-291 (1995).
31. Dillon KB, Platt AWG, Waddington TC. The identification of some new azido-derivatives of phosphorus. *Inorg. Nucl. Chem. Letters* **14**, 511-513 (1978).
32. Buder W, Schmidt A. Phosphorazide und deren Schwingungsspektren. *Z. Anorg. Allg. Chem.* **415**, 263-267 (1975).
33. Gilyarov VA. Phosphorus Acid Azides. *Russ. Chem. Rev.* **51**, 909-920 (1982).
34. Holleman AF. *Lehrbuch der anorganischen Chemie*. Walter de Gruyter GmbH & Co KG, 2019.
35. Dielmann F, Back O, Henry-Ellinger M, Jerabek P, Frenking G, Bertrand G. A Crystalline Singlet Phosphinonitrene: A Nitrogen Atom–Transfer Agent. *Science* **337**, 1526 (2012).
36. Staudinger H, Meyer J. Über neue organische Phosphorverbindungen III. Phosphinmethylenderivate und Phosphinimine. *Helv. Chim. Acta* **2**, 635-646 (1919).
37. Transue WJ, Velian A, Nava M, García-Iriepa C, Temprado M, Cummins CC. Mechanism and Scope of Phosphinidene Transfer from Dibenzo-7-phosphanorbornadiene Compounds. *J. Am. Chem. Soc.* **139**, 10822-10831 (2017).
38. Hamon P, Toupet L, Roisnel T, Hamon J-R, Lapinte C. Preparation and Characterization of the Triflate Complex [Cp*(dppe)$FeOSO_2CF_3$]: A Convenient Access to Labile Five- and Six-Coordinate Iron(I) and Iron(II) Complexes. *Eur. J. Inorg. Chem.* **2020**, 84-93 (2020).
39. Huber K-P. *Molecular spectra and molecular structure: IV. Constants of diatomic molecules*. Springer Science & Business Media, 2013.
40. Knizia G. Intrinsic Atomic Orbitals: An Unbiased Bridge between Quantum Theory and Chemical Concepts. *J. Chem. Theory Comput.* **9**, 4834-4843 (2013).
41. Niecke E, Detsch R, Nieger M, Reichert F, Schoeller W. From covalent to ionic bonding: spontaneous bond dissociation in oxy-substituted iminophosphanes. *Bull. Soc. Chim. Fr.* **130**, 25-31 (1993).
42. Kraka E, Freindorf M. Characterizing the Metal–Ligand Bond Strength via Vibrational Spectroscopy: The Metal–Ligand Electronic Parameter (MLEP). In: Lledós A, Ujaque G (eds). *New Directions in the Modeling of Organometallic Reactions*. Springer International Publishing: Cham, 2020, pp 227-269.
43. Prisecaru I. WMOSS4 Mößbauer Spectral Analysis Software. 2009-2016 [cited 08/24/2021]Available from: www.wmoss.org.
44. Rittle J, Peters JC. Fe–N_2/CO complexes that model a possible role for the interstitial C atom of FeMo-cofactor (FeMoco). *Proc. Natl. Acad. Sci. USA* **110**, 15898 (2013).
45. Latypov SK, Polyancev FM, Yakhvarov DG, Sinyashin OG. Quantum chemical calculations of ^{31}P NMR chemical shifts: scopes and limitations. *Phys. Chem. Chem. Phys.* **17**, 6976-6987 (2015).
46. Schneider WB, Bistoni G, Sparta M, Saitow M, Riplinger C, Auer AA*, et al.* Decomposition of Intermolecular Interaction Energies within the Local Pair Natural Orbital Coupled Cluster Framework. *J. Chem. Theory Comput.* **12**, 4778-4792 (2016).
47. Mitoraj MP, Michalak A, Ziegler T. A Combined Charge and Energy Decomposition Scheme for Bond Analysis. *J. Chem. Theory Comput.* **5**, 962-975 (2009).
48. Altun A, Neese F, Bistoni G. Effect of Electron Correlation on Intermolecular Interactions: A Pair Natural Orbitals Coupled Cluster Based Local Energy Decomposition Study. *J. Chem. Theory Comput.* **15**, 215-228 (2019).

49. Stanford University Environmental Health & Safety. Information on Azide Compounds. [cited 08/24/2021] https://ehs.stanford.edu/reference/information-azide-compounds.
50. Pangborn AB, Giardello MA, Grubbs RH, Rosen RK, Timmers FJ. Safe and Convenient Procedure for Solvent Purification. *Organometallics* **15**, 1518-1520 (1996).
51. Williams DBG, Lawton M. Drying of Organic Solvents: Quantitative Evaluation of the Efficiency of Several Desiccants. *J. Org. Chem.* **75**, 8351-8354 (2010).
52. Roger C, Hamon P, Toupet L, Rabaa H, Saillard JY, Hamon JR*, et al.* Halo- and alkyl(pentamethylcyclopentadienyl)[1,2-bis(diphenylphosphino)ethane]iron(III) 17-electron complexes: synthesis, NMR and magnetic properties and EHMO calculations. *Organometallics* **10**, 1045-1054 (1991).
53. Patel D, Wooles A, Cornish AD, Steven L, Davies ES, Evans DJ*, et al.* Synthesis and characterisation of halide, separated ion pair, and hydride cyclopentadienyl iron bis(diphenylphosphino)ethane derivatives. *Dalton Trans.* **44**, 14159-14177 (2015).
54. Fulmer GR, Miller AJM, Sherden NH, Gottlieb HE, Nudelman A, Stoltz BM*, et al.* NMR Chemical Shifts of Trace Impurities: Common Laboratory Solvents, Organics, and Gases in Deuterated Solvents Relevant to the Organometallic Chemist. *Organometallics* **29**, 2176-2179 (2010).